Separation Science and Technology
Publication details, including instructions for authors and subscription information:
http://www.informaworld.com/smpp/title~content=t713708471

Migration and Deposition of Submicron Particles in Crossflow Microfiltration

Kuo-Jen Hwang[a]; Mei-Chou Yu[a]; Wei-Ming Lu[b]
[a] DEPARTMENT OF CHEMICAL ENGINEERING TAMKANG, UNIVERSITY TAMSUI, TAIPEI HSIEN, TAIWAN, REPUBLIC OF CHINA [b] DEPARTMENT OF CHEMICAL ENGINEERING, NATIONAL TAIWAN UNIVERSITY, TAIPEI, TAIWAN, REPUBLIC OF CHINA

To cite this Article Hwang, Kuo-Jen , Yu, Mei-Chou and Lu, Wei-Ming(1997) 'Migration and Deposition of Submicron Particles in Crossflow Microfiltration', Separation Science and Technology, 32: 17, 2723 — 2747
To link to this Article: DOI: 10.1080/01496399708002219
URL: http://dx.doi.org/10.1080/01496399708002219

SEPARATION SCIENCE AND TECHNOLOGY, **32**(17), pp. 2723–2747, 1997

Migration and Deposition of Submicron Particles in Crossflow Microfiltration

KUO-JEN HWANG* and MEI-CHOU YU
DEPARTMENT OF CHEMICAL ENGINEERING
TAMKANG UNIVERSITY
TAMSUI, TAIPEI HSIEN, TAIWAN 25137, REPUBLIC OF CHINA

WEI-MING LU
DEPARTMENT OF CHEMICAL ENGINEERING
NATIONAL TAIWAN UNIVERSITY
TAIPEI, TAIWAN 10617, REPUBLIC OF CHINA

ABSTRACT

The migration and deposition of submicron particles in laminar crossflow microfiltration is simulated by integrating the Langevin equation. The effects of operating conditions on the particle trajectories are discussed. It is found that the Brownian motion of particles plays an important role in particle migration under a smaller crossflow velocity of suspension or a smaller filtration rate. Based on the simulated trajectories of particles, the transported flux of particles arriving at the membrane surface can be estimated. The particle flux increases with an increase of filtration rate and with a decrease of particle diameter; however, the effect of crossflow velocity on the particle flux is not obvious. The forces exerted on particles are analyzed to estimate the probability of particle deposition on the membrane surface. The probability of particle deposition increases with an increase of filtration rate, with a decrease of crossflow velocity, with a decrease of particle diameter, or with an increase of zeta potential on the particle surfaces. The simulated results of packing structures of particles on the membrane surface at the initial stage of filtration show that a looser packing can be found under a larger crossflow velocity, a smaller filtration rate, or a smaller diameter of filtered particles. Crossflow microfiltration experiments are carried out to demonstrate the reliability of the proposed theory. The deviation between the predicted and experimental data of filtration rate at the initial period of filtration is less than 10% when the Reynolds number of the suspension flow ranges from 100 to 500.

* To whom correspondence should be addressed.

Key Words. Crossflow microfiltration; submicron particles; filtration; Particle migration; Particle deposition

INTRODUCTION

Crossflow microfiltration is increasingly used in many industries for separation of submicron particles from liquids. The performance of a filtration is determined by several major factors, such as the Brownian motion of particles, electrostatic interaction between particles, and hydrodynamics, etc., but this complex course has not yet been well investigated.

Various polarization models have been proposed to describe the phenomena of concentration polarization and physical fouling in ultrafiltration (1). At steady state, the particle flux convected toward the filter membrane was balanced by that diffused away from the membrane. However, the predicted flux for micron-sized particles was found to be one or more orders of magnitude less than those of experimental data if the Stokes–Einstein relationship was used as the Brownian diffusivity. Green and Belfort (2) referred to this discrepancy as the "flux paradox for colloidal suspensions." To resolve this, Zydney and Colton (3) proposed that the concentration polarization model could be applied to microfiltration of micron-sized and larger particles if the Brownian diffusivity was replaced by the shear-induced hydrodynamic diffusivity.

For the crossflow filtration of particles with a diameter of 0.1–10 μm, the resistance of the formed filter cake will play the major role in the performance of filtration. Since the cake resistance is mainly determined by the amount and the structure of the filter cake, to understand how the particles migrate and arrive at the membrane surface and what structure will be constructed are the essential steps in grasping the problem of filtration.

For crossflow filtration of micron particles, Altena and Belfort (4) used the hydrodynamic model to analyze the flow field of fluid and the trajectories of particles in a crossflow filter. The concentration profile and the transport flux of particles arriving at the membrane surface can then be calculated accordingly. On the other hand, the selective deposition of particles in crossflow filtrations has been discussed (5, 6). Whether or not a particle arriving at the membrane surface can deposit stably is determined by the external forces exerted on it. By using a force balance model, Lu and Hwang (7) calculated the critical angle of friction between micron particles staying on the cake surface in a crossflow filtration system. The critical value of the frictional angle can be used for predicting the probability of particle deposition and for simulating the packing structure of parti-

cles on the cake surface by using their proposed model. However, the effects of the Brownian motion of particles and the interactions of particles were not considered in these previous research efforts.

The Brownian dynamic simulation method has been well used to simulate the migration of colloids in a flowing system. The particle trajectories can be traced by using Newton's second law of motion. Ansell and Dickinson (8) discussed the effects of colloidal and hydrodynamic interaction between particles on the sediment structure by using this method. They concluded that a more compact structure of sediment was constructed if Brownian motion of particles was considered. Recently, Ansell and Dickinson (9, 10) extended the method of Brownian dynamic simulation to study the kinetics of colloidal coagulation in a simple shear flow. This method has also been used to study how aerosol deposits onto a spherical collector (11). In recent years, Lu et al. (12) simulated the structures of filter cake formed in constant pressure cake filtrations by using the Brownian dynamic simulation method. Analyses of the effects of Brownian motion, frictional force, van der Waals force, and electrostatic force on the cake structure revealed that the most compact cake was formed when the frictional drag and Brownian force are of the same order of magnitude.

In this article a numerical program based on the Langevin equation is designed to trace the loci of submicron particles in crossflow microfiltration. The deposition of particles on the filter medium is also simulated by using force balance on particles. The porosity of the packed structure at the initial stage of filtration can then be estimated accordingly.

SIMULATION METHOD

Trajectories of Particles in Filter

Figure 1 shows the phenomenon of particle migration in a two-parallel-plate crossflow microfilter and defines the coordinates used in this analysis. For an incompressible spherical particle, the Langevin equation of motion can be written as

$$m_p \frac{dv_p}{dt} = F_d + F_g + F_l + F_i + F_B \tag{1}$$

where m_p is the mass of the particle, v_p is the velocity of the particle, t is time, and F_d, F_g, F_l, F_i, and F_B are the frictional drag, net gravity, inertial lift force, net interparticle force, and Brownian force, respectively. Each term in the above equation should be analyzed prior to obtaining the instantaneous velocity of the particle or to estimating the displacement of the particle in a time increment.

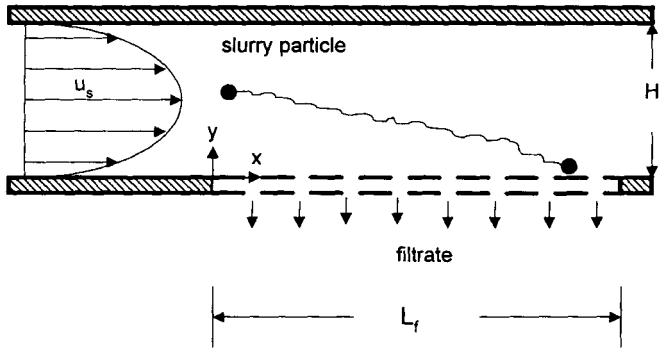

FIG. 1 A schematic diagram of the crossflow microfilter.

Drag Due to Fluid Flow, F_d

The frictional drag exerted on a spherical particle is determined by the local flow field of fluid and can be divided into two components whose directions are either parallel or vertical to the crossflow of suspension.

F_{dx}. If the deviation between the velocities of fluid and the particles is very small, the drag exerted on a particle in the x-direction can be estimated by Stokes' law, that is,

$$F_{dx} = 3\pi\mu d_p(u_x - v_{px}) \tag{2}$$

where d_p is the diameter of the particle while u_x and v_{px} are the velocities of fluid and the particle in the x-direction, respectively. Since the Reynolds number of permeating flow is very small for most crossflow microfiltrations, the variation of crossflow velocity can be neglected. Therefore, the fully developed profile of u_x is parabolic for a laminar crossflow and can be given by

$$u_x = 6u_s\left[\left(\frac{y}{H}\right) - \left(\frac{y}{H}\right)^2\right] \tag{3}$$

where u_s is the average crossflow velocity at the inlet of the filter.

F_{dy}. The frictional drag exerted on the particle in the y-direction can be expressed as

$$F_{dy} = 3\pi\mu d_p(u_y - v_{py})\phi \tag{4}$$

where ϕ is the correction factor for a permeating boundary. If the location of the particle is very near the formed cake or the filter medium, the value

of ϕ can be estimated by the results of Sherwood (13). Since the Reynolds number of permeating flow is very small, the variation of u_y in the x-direction can be neglected, and the fully developed profile of u_y can be given by the perturbation method (14), that is,

$$u_y = q\left[1.5\left(1 - \frac{y}{H}\right) - 0.5\left(1 - \frac{y}{H}\right)^3\right] \tag{5}$$

where q is the quasi-stationary filtration rate.

Inertial Lift Force

Extending the results of Vasseur and Cox (15), the inertial lift velocity of a particle can be given by

$$v_l = \left(\frac{61}{576\nu}\right)\left(\frac{\tau_w}{\mu}\right)^2\left(\frac{d_p}{2}\right)^3 \tag{6}$$

where τ_w is the shear stress acting on the wall of the filter, while ν is the kinematic viscosity of fluid.

Net Gravity Force, F_g

The net gravity force exerted on a submerged particle can be given by

$$F_g = \frac{\pi}{6}(\rho_s - \rho)g d_p^3 \tag{7}$$

Interparticle Force, F_i

The DLVO theory is adopted for estimating the interparticle forces in this study. This theory concluded that there are two major long-range colloidal interactions, such as electrostatic force, F_e, and van der Waals force, F_v, between two approaching particles, and that the net interparticle force can be given by summing these forces as

$$F_i = F_v + F_e \tag{8}$$

In this study the contributions from neighboring particles are added on the basis of linear superposition. These forces are analyzed below.

Van der Waals Force. Considering two equal-sized neighboring particles with radius a, the van der Waals potential between them can be estimated from (16)

$$V_v = \frac{A_H a}{12D}\left[1 - \frac{bD}{\lambda}\ln\left(1 + \frac{\lambda}{bD}\right)\right] \tag{9}$$

where A_H is the Hamaker constant, D is the shortest distance between the particle surfaces, λ is the characteristic wavelength for the interaction which is often assumed to be about 100 nm (16), and the constant b is equal to 5.32 if D is smaller than a (16).

The van der Waals force between two spherical particles can then be calculated by

$$F_v = -\frac{\partial V_v}{\partial D} = -\frac{A_H a}{12D^2}\left(1 - \frac{1}{1 + \lambda/bD}\right) \tag{10}$$

Electrostatic Force. *(i) The thickness of the electric double layer is much smaller than a.*

For low surface potentials, the repulsive electric energy between equal-sized particles with radius a under the condition of constant surface charge is given by (17)

$$V_e = -2\pi e_0 e_r a \Psi_0^2 \ln[1 - \exp(-\kappa D)] \tag{11}$$

where e_0 ($= 8.85 \times 10^{-12}$ $C^2 \cdot J^{-1} \cdot m^{-1}$) is the absolute permittivity of free space, e_r is the dielectric constant of the fluid between particles, Ψ_0 is the Stern potential, and κ is the reciprocal of the thickness of the double layer.

(ii) The thickness of the electric double layer is much larger than a. The repulsive electrostatic energy between equal-sized particles can be given as (17)

$$V_e = \pi e_0 e_r \frac{d_p^2}{(D + d_p)} \Psi_0^2 \exp(-\kappa D) \tag{12}$$

Then Eq. (11) or (12) can be differentiated with respect to D to obtain the electrostatic force between two equal-sized spherical particles. In general, the value of Ψ_0 cannot be measured from experiments. The measurable value, the zeta potential, ζ, has thus been the most widely used. As the values of ζ, e_r, κ, and D are known, the value of electrostatic force, F_e, can be estimated.

Once the values of F_v and F_e are obtained, F_i can be calculated from Eq. (8).

Brownian Force, F_B

F_B is a random force due to particle collisions with the surrounding fluid molecules and can be expressed as

$$F_B = m_p A(t) \tag{13}$$

where $A(t)$ is the Brownian random force exerted on per unit mass of the particle, and it follows a Gaussian distribution. Therefore, a sequence of

random numbers with Gaussian distribution can be generated by a computer to determine F_B.

By defining the following dimensionless variables,

$$x^* = \frac{x}{d_p}, \; y^* = \frac{y}{d_p}, \; u_x^* = \frac{u_x}{u_s}, \; u_y^* = \frac{u_y + v_l}{u_s}, \; r^* = \frac{r}{d_p}, \; t^* = \frac{u_s t}{d_p} \tag{14}$$

the equation of motion, Eq. (1), can be rearranged as

$$\frac{d^2 r^*}{dt^{*2}} + \frac{1}{C_1}\frac{dr^*}{dt^*} = F(x^*, y^*) + \frac{d_p}{u_s^2} A(t) \tag{15}$$

where $r^* \; (= x^* \vec{i} + y^* \vec{j})$ is the position vector of the particle, and

$$F(x^*, y^*) = F_x^* \vec{i} + F_y^* \vec{j}$$

$$F_x^* = \frac{1}{C_1}\left(u_x^* + \frac{1}{C_2} F_{i,x}\right)$$

$$F_y^* = \frac{1}{C_1}\left(u_y^* + \frac{1}{C_2} F_{i,y} + C_3\right)$$

in which

$$C_1 = \frac{\rho_s u_s d_p}{18\mu\phi}, \qquad C_2 = 3\pi\mu d_p \phi, \qquad C_3 = \frac{(\rho_s - \rho) g d_p^2}{18\mu u_s \phi}$$

and $F_{i,x}$ and $F_{i,y}$ are the x-component and y-component of the net interparticle force, respectively. By multiplying $\exp(t^*/C_1)$ for each term and integrating Eq. (15) once from $t^* = 0$ to $t^* = t^*$, an expression for velocity can be obtained as

$$v^* - v_0^* \exp(-t^*/C_1) = \exp(-t^*/C_1) \int_0^{t^*} F(x^*, y^*) \exp(\tau/C_1) d\tau + \frac{d_p}{u_s^2} \exp(-t^*/C_1) \int_0^{t^*} A(\tau) \exp(\tau/C_1) d\tau \tag{16}$$

where $v_0^* \; (= v_0/u_s)$ is the dimensionless velocity of the particle at $t = 0$. If the time increment is small enough such that the force $F(x^*, y^*)$ remains constant in the time interval, the above equation can be integrated once again to obtain the particle displacement as

$$r^* - r_0^* - C_1 v_0^* [1 - \exp(-t^*/C_1)] = C_1 F(x^*, y^*)\{t^* - C_1[1 - \exp(-t^*/C_1)]\} + \frac{d_p C_1}{u_s^2} \int_0^{t^*} A(\tau)\{1 - \exp[-(t^* - \tau)/C_1]\} d\tau \tag{17}$$

where r_0 is the initial particle position. According to the analysis of Gupta and Peter (11), the integration

$$R_1(t^*) = \int_0^{t^*} A(\tau) \exp[-(t^* - \tau)/C_1]d\tau \tag{18}$$

and

$$R_2(t^*) = \int_0^{t^*} A(\tau)\{1 - \exp[-(t^* - \tau)/C_1]\}d\tau \tag{19}$$

follow a bivariate Gaussian distribution with the following statistical properties:

$$E[R_1(t^*)] = E[R_2(t^*)] = 0 \tag{20}$$

$$E[R_1(t^*)R_2(t^*)] = C_1 \frac{3kT}{m}[1 - \exp(-t^*/C_1)]^2 \tag{21}$$

$$\sigma^2_{R_1(t^*)} = \frac{3kT}{m}[1 - \exp(-2t^*/C_1)] \tag{22}$$

$$\sigma^2_{R_2(t^*)} = C_1^2 \frac{3kT}{m}\left[\frac{2t^*}{C_1} - 3 + 4\exp(-t^*/C_1) - \exp(-2t^*/C_1)\right] \tag{23}$$

Therefore, the velocities and trajectories of particles in the crossflow microfilter can be simulated in accord with Eqs. (16) and (17).

Particle Flux Arriving at Filter Membrane

Since the filtration rate is far slower than the crossflow velocity for most microfiltrations, only those particles whose initial locations are very near the membrane surface can be transported to the membrane surface before they leave the filter. The notation y_b is defined as the coordinate of entering particles below which particles will be transported to the membrane surface. For a given operating condition, the value of y_b can be obtained by guessing it from the membrane surface and proceeding with the above simulation until particles cannot be transported to the membrane surface. Therefore, the transport flux of particles arriving at the membrane surface can be estimated by

$$N_b = \frac{1}{L_f}\int_0^{y_b} C_0 u_x dy \tag{24}$$

where C_0 is the concentration of suspension. In this study, the profile of C_0 is assumed to be uniform in the inlet of the filter.

Deposition of Particles on Filter Membrane

During a course of crossflow filtration, particles are transported, arrive at the surface of the membrane, and deposit to form a filter cake or a concentration polarization layer flowing near the membrane. Whether a particle can deposit stably or not is determined by the forces exerted on the particle. Figure 2 depicts a filtration system near a filter membrane, where Particle B is a metastable particle while Particle A is a particle just arriving at the cake surface that comes into contact with Particle B. Each force or drag exerted on the particle has been analyzed in the previous section. The notations F_1 and F_2 shown in the figure are the components of the net force whose directions are vertical and parallel to the line connecting with the gravity centers of the particles, respectively. In this study the force analysis for the particles are adopted to determine whether a particle will deposit on the touched point or migrate to another stable position. The modes of particle migration are discussed below.

Drag Force Far Larger Than Interparticle Force

In the case the drag force is dominant and exceeds the maximum repulsive force between the particles, which causes Particle A to nearly touch

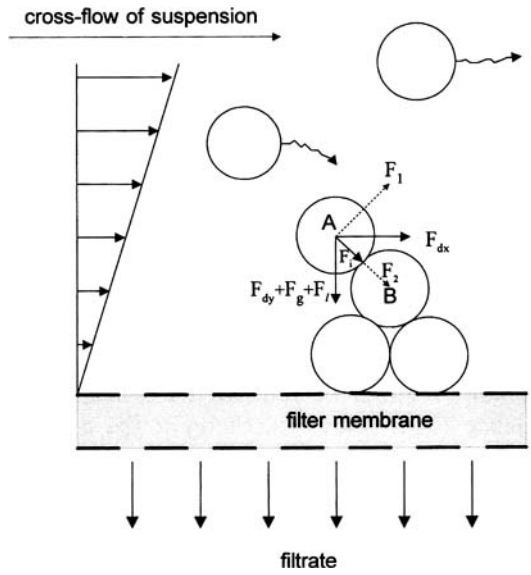

FIG. 2 Forces exerted on a depositing particle in a crossflow microfiltration system.

the surface of Particle B. The shortest distance between the particles is assumed to be two times the thickness of the Stern layer due to its compact matter (16). In such a situation the migration of particles is determined by the external forces and the friction between particles. The analyses proposed by the authors (7) can be employed to determine the stability of Particle A. If the frictional angle is smaller than its critical value, the friction between particles is large enough to cause the particle to stick stably on the contact point; otherwise, Particle A will reenter the bulk flow of suspension.

Drag Force Smaller Than Interparticle Force

If the maximum repulsive force between particles is larger than the net force of other forces in the same direction, there will exist an equilibrium of separate distances between particles. The particles cannot actually come into contact with each other, and there is no net force acting in the direction parallel to the connecting line between the two gravity centers of the particles. For this case, if F_1 is not equal to zero, Particle A will still migrate due to the lubricant effect of the double layer, and the direction of particle migration will be according to the direction of F_1. When the value of F_1 is positive (the direction shown in Fig. 2), Particle A will leave the original position and reenter the bulk flow of suspension. When the value of F_1 is negative, Particle A will move into the pore of the filter cake until it simultaneously touches more than one particle.

When a transported particle has arrived at the membrane or cake surface, whether it can deposit to form a cake or reenter the bulk flow of suspension should be recorded in order to obtain the probability of particle deposition.

Simulation Procedures

The time increment used should be larger than the momentum relaxation time, $m_p/3\pi\mu d_p$ (16); however, it must be small enough to neglect the variations of external forces in each time interval. Thus, a time increment equal to 1×10^{-5} s was chosen in this study.

The instantaneous number of generated particles was determined by the particle balance for the slurry arriving at the cake surface, and the initial coordinations of particles were determined by a numerical generator with a random distribution function.

According to the simulation procedures described in the previous sections, the migration and deposition of particles could be simulated by a similar scheme of Lu et al. (12). After a period of simulation, the filter cake was divided into several layers to estimate the local and average porosity of the cake (12).

EXPERIMENTAL

Figure 3 shows the schematic diagram of the crossflow microfiltration system. A two-parallel-plate crossflow filter with a filter channel of 4.5 $\times$ 10^{-4} m height, 6.3 $\times$ 10^{-2} m length, and 7.3 $\times$ 10^{-3} m width was used to carry out the experiments. Thus the filtration area was 4.6 $\times$ 10^{-4} m^2. Three uniform-sized PMMA (polymethyl methacrylate) particles with diameters of 0.25, 0.4, and 0.8 μm, respectively, and with a density of 1210 kg/m^3 were suspended in deionized water at 20°C to prepare the suspensions. The pH value of the suspension was 5.5, and the zeta potential of the particles was −25.0 mV. The friction coefficient between PMMA particles in water was measured as 0.77. The crossflow velocities used had a range of 0.2–0.6 m/s. As a result, the Reynolds number of the suspension flow ranged from 100 to 500. The filter membrane was made of polyvinylidene fluoride (PVDF) with an average pore diameter of 0.2 μm, and its filtration resistance was 1.12 $\times$ 10^{10} m^{-1}.

In each experiment the crossflow velocity and the filtration pressure were adjusted to the setting value by the control valves. The temperature was kept at 20°C by using a water bath. The filtration rate was detected by a load cell and recorded on a personal computer. The concentrate was recycled back to the suspension tank, and deionized water was added continuously into the tank to keep the concentration constant.

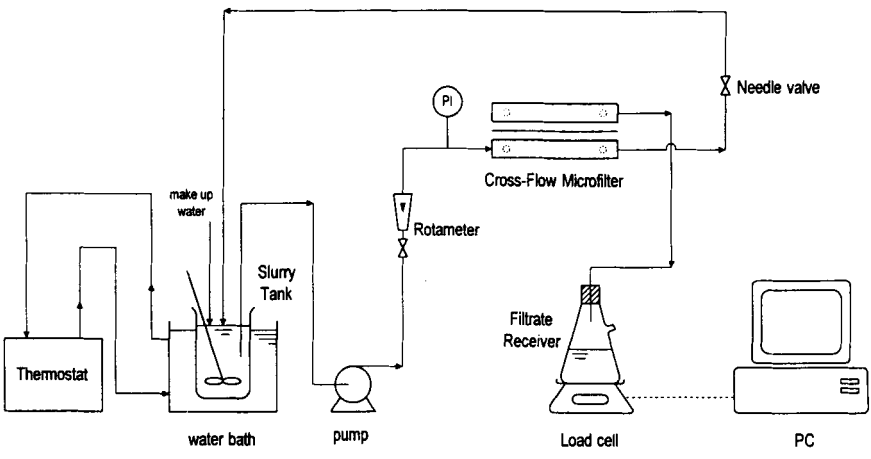

FIG. 3 A schematic diagram of crossflow microfiltration system.

RESULTS AND DISCUSSION

Particle Trajectories

Figures 4–7 show examples of the simulated trajectories of submicron particles with different sizes under different conditions. The value of L_f is set to 0.1 m for these simulation. All of the original locations of particles are set at the same point (i.e., $x = 10^{-5}$ m, $y = 10^{-6}$ m) except in Fig. 4. Figure 4 depicts the trajectories of submicron particles with a diameter of 0.4 μm for three different inlet heights. The results shown in the figure demonstrate that only those particles whose inlet heights are very near the filter membrane have opportunities to arrive at the membrane surface. Since the order of magnitude of the filtration rate is far smaller than that of the crossflow velocity, the filtration rate has no significant impact on the trajectories of most particles far from the membrane in the filter. From Figs. 5 and 6 it can be noticed that more Brownian motions of particles can be observed for a slower flow rate of filtrate or crossflow velocity of suspension. A decreasing crossflow velocity or an increasing filtration rate will increase the migrating distance in the x-direction of particles before they arrive at the membrane surface, which implies that the inlet particles have more opportunities to arrive at the membrane surface under those conditions. Figure 7 shows how the particle size affects the migration of particles. It can be found that the smaller the particle is, the more intense the random walk of the particle will be. Moreover, the distance

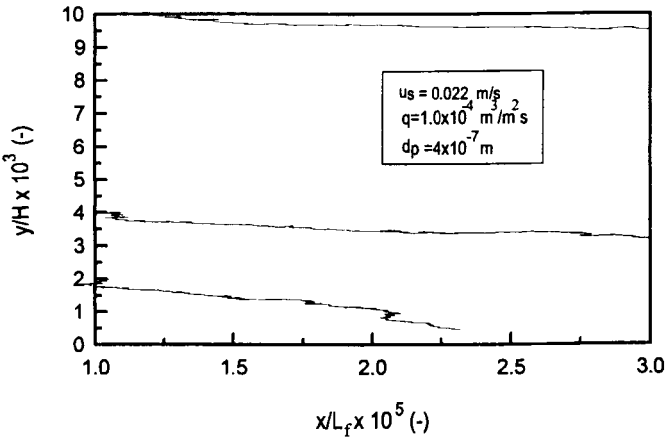

FIG. 4 Trajectories of submicron particles with different inlet heights.

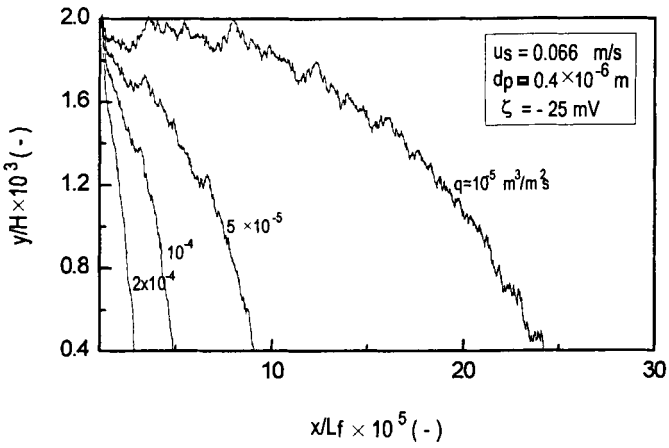

FIG. 5 Trajectories of submicron particles under various filtration rates.

in which the smaller particle migrates in the x-direction is shorter. This fact implies that the value of y_b would be larger for filtering smaller particles.

Transported Flux of Particles Arriving at Membrane Surface

Figure 8 shows the transported flux of particles arriving at the membrane surface, N_b, under various filtration rates for three different

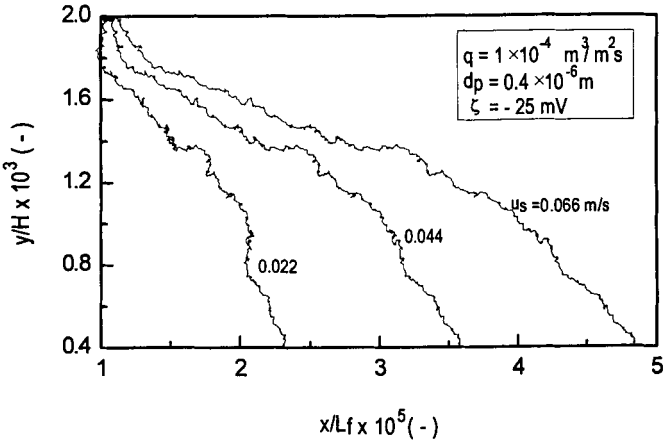

FIG. 6 Trajectories of submicron particles under various crossflow velocities.

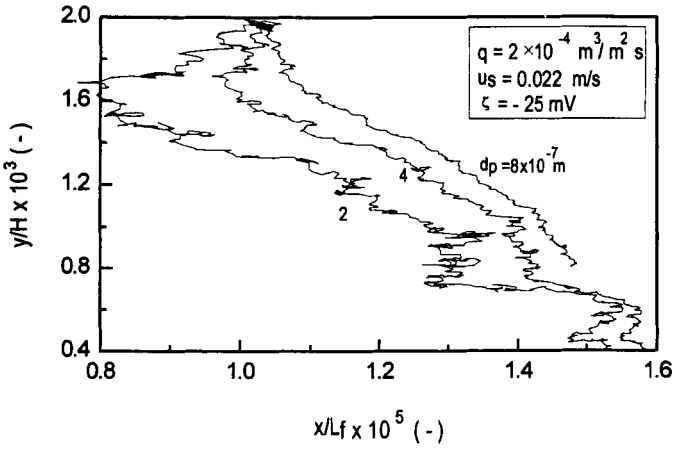

FIG. 7 Effect of particle size on the trajectory of submicron particles.

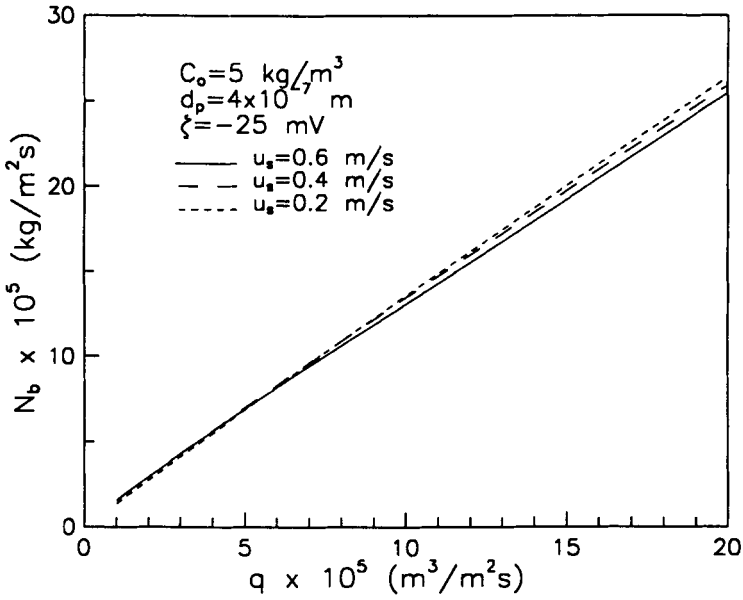

FIG. 8 Effect of filtration rate on the transported flux.

crossflow velocities. The values of N_b are calculated by using Eq. (24). Since particles are easily transported to the membrane surface under a smaller crossflow velocity or a larger filtration rate (see Figs. 5 and 6), one can notice from the figure that N_b increases with an increase of the filtration rate. However, for a given value of q, the effect of u_x on the value of N_b is not significant. For a large q, the smaller the value of u_x, the larger the amount of N_b will be because a smaller u_x will result in a larger value of y_b. That is, N_b may increase with a decrease of u_x. However, this tendency is reversed under a small value of q. This may be because a larger amount of particles is transported in the x-direction for a larger value of u_x.

Figure 9 illustrates the effect of particle diameter on the value of N_b. For a given operating condition, the value of N_b will decrease with an increase of particle diameter. This can be expected since the Brownian motion of smaller particles will result in a larger value of y_b. Furthermore, since an increase of u_x will decrease the value of y_b, the value of N_b will decrease accordingly.

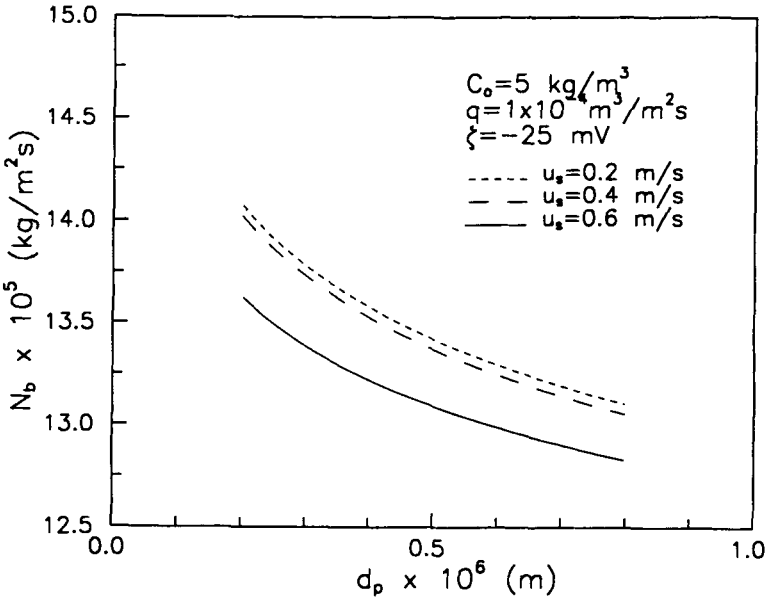

FIG. 9 Effect of particle diameter on the transported flux.

Probability of Particle Deposition

Figure 10 illustrates how the operating conditions affect the probability of particle deposition. This figure shows that the probability will increase with an increase of filtration rate or a decrease of crossflow velocity. These results are the same as those of previous research studies (5–7), perhaps because the ratio of F_{dy} to F_{dx} will increase under those conditions. It can be found that P attains 100% as $q > 7 \times 10^{-5}$ m^3/m^{2}s under $u_x = 0.2$ m/s, which means that particles arriving at the membrane surface can deposit immediately.

The effect of particle diameter on the probability of particle deposition is shown in Fig. 11. For a given value of ζ, the value of P will decrease with an increase of particle diameter. This result is the same as those of previous research efforts (5–7) and implies that a smaller particle will remain more stably on the membrane surface than will a larger one.

Figure 12 shows the effect of particle zeta potential on the probability of particle deposition. Since the amount of frictional drag is larger than that of interparticle force under most operating conditions in this study, the depositing particles can come into contact with each other. It can be expected that the friction between particles will play a major role in particle deposition. From this figure it can be found that the value of P will increase with an increase of zeta potential. This is because a larger value of ζ will result in a larger repulsive force between particles, which causes the friction between particles to decrease. For the case of $u_x = 0.2$ m/s, the value of P is equal to 100% within the range of $\zeta = -20$ to -60 mV.

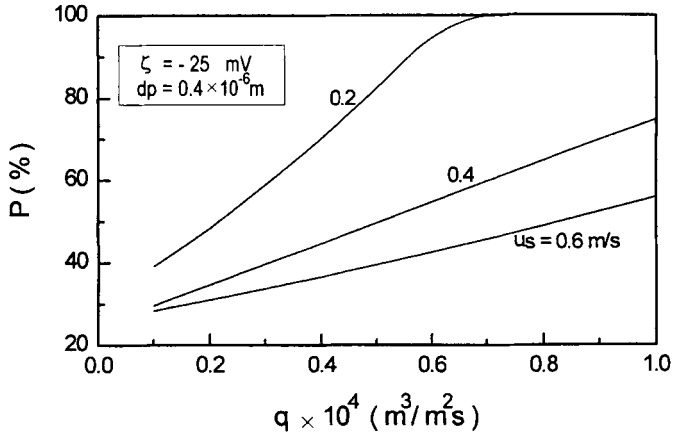

FIG. 10 Effect of filtration rate on the probability of particle deposition.

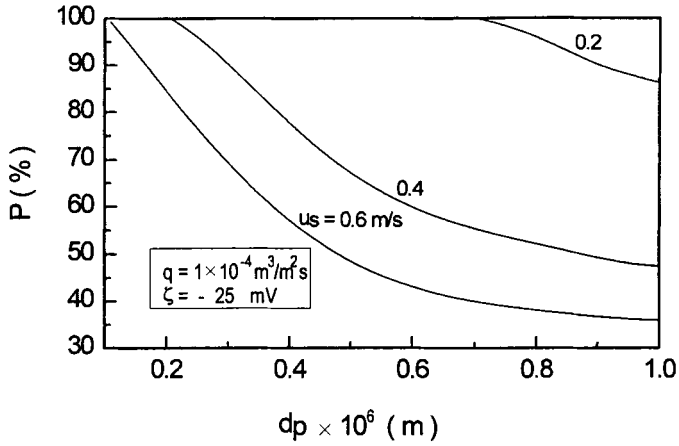

FIG. 11 Effect of particle diameter on the probability of particle deposition.

Packing Structure of Particles on Membrane

Figure 13 shows the packing structures of particles on the membrane surface for a given filtration rate under various crossflow velocities. It can be found that particles are packed with an angle with respect to the direction of filtration due to the tangential flow of suspension. However, this phenomenon is not as obvious as that in crossflow filtration of micron

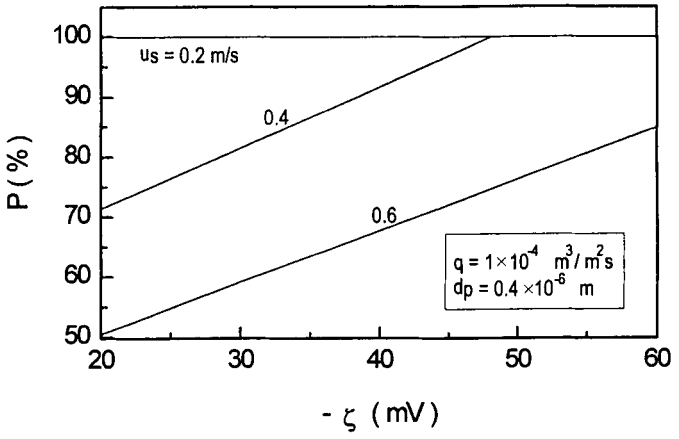

FIG. 12 Effect of zeta potential on the probability of particle deposition.

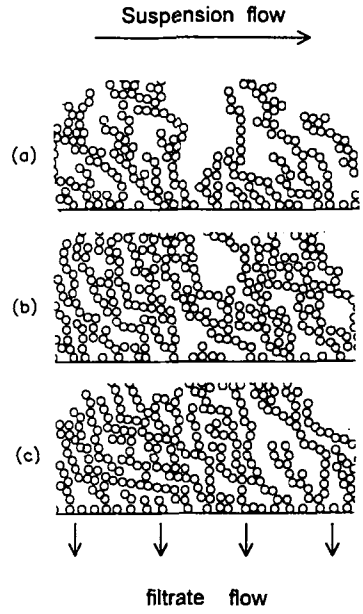

FIG. 13 Packing structures of submicron particles on the membrane surface under various crossflow velocities at $q = 1.0 \times 10^{-4}$ m^3/m^2·s (a) $u_x = 0.4$ m/s; (b) $u_x = 0.2$ m/s; (c) $u_x = 0.1$ m/s.

particles (7) because of the existence of Brownian motion of submicron particles. Since a decrease of crossflow velocity will increase the opportunities for particles to stick on or roll down within the cake, a more compact cake was constructed as shown in the figure.

Another comparison of particle packing is shown in Fig. 14. For a given velocity of crossflow, a larger filtration rate will increase the stability of particles staying on the membrane surface. As a result, a more compact structure will be packed under a larger filtration rate.

Porosity of Cake

Figure 15 illustrates how the crossflow velocity affects the porosity on the cake surface. The regressed line shows that the packing porosity will increase with an increase of the crossflow velocity of suspension. This is the same as in crossflow filtration of micron particles (7). Past research has shown that increasing the crossflow velocity results in the formation of a finer and higher specific-resistance cake when polydispersed particles

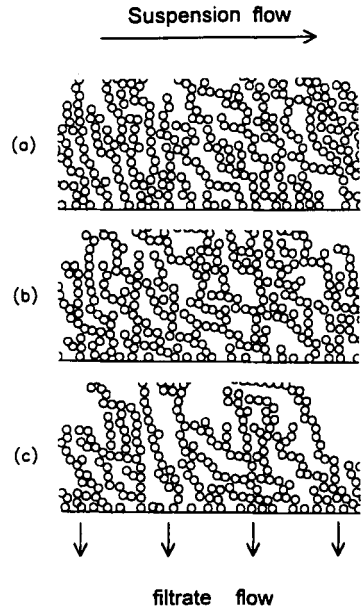

FIG. 14 Packing structures of submicron particles on the membrane surface under various filtration rates at $u_x = 0.2$ m/s. (a) $q = 2.0 \times 10^{-4}$ m^3/m^2·s; (b) $q = 1.0 \times 10^{-4}$ m^3/m^2·s; (c) $q = 0.5 \times 10^{-4}$ m^3/m^2·s.

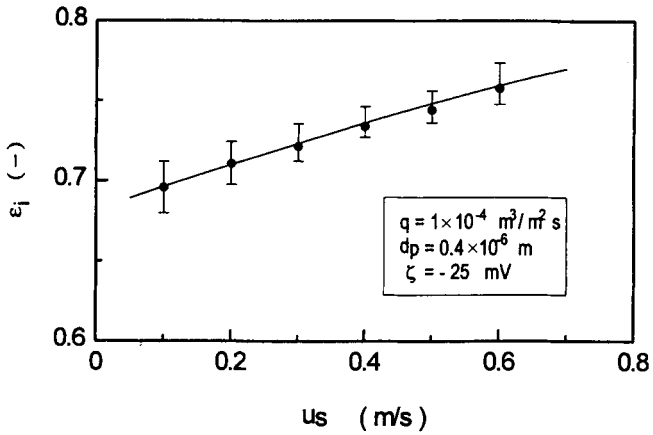

FIG. 15 Simulated packing porosity of particles under various crossflow velocities.

are filtered, e.g., Lu and Ju (6). However, the effect of cake porosity, another important factor, on filtration resistance is rarely discussed. Figure 15 shows that the porosity of a cake may vary with the crossflow velocity even if uniform-sized particles are filtered.

Figure 16 illustrates the effect of the filtration rate on cake porosity. Since a higher filtration rate will cause the depositing particles to more easily roll down within the filter cake toward the membrane, the packing porosity will decrease with an increase of filtration rate.

Figure 17 is a plot of ϵ_i vs d_p. Since the Brownian motion is more significant, the separation distance between neighboring particles in the cake is larger, and the critical angle of friction is smaller (7) for smaller particles, so a looser packing will be constructed (12). Thus, the value of ϵ_i will decrease with an increase of d_p, as shown in the figure.

In order to demonstrate the reliability of the proposed theory, crossflow microfiltrations were carried out to obtain the filtration rate at the initial period of filtration. A comparison between the predicted results and the experimental data is summarized in Table 1. From the results shown, there is agreement between the calculated results and the experimental data except for the case of run number 4. Since the size of particles used is larger in this case, the lower specific filtration resistance and the higher filtration rate may result in a further compression of the cake at the beginning of filtration. As a result, the experimental filtration rate is smaller than the predicted value. However, the deviations between predictions and experimental data of the filtration rate are less than 10%.

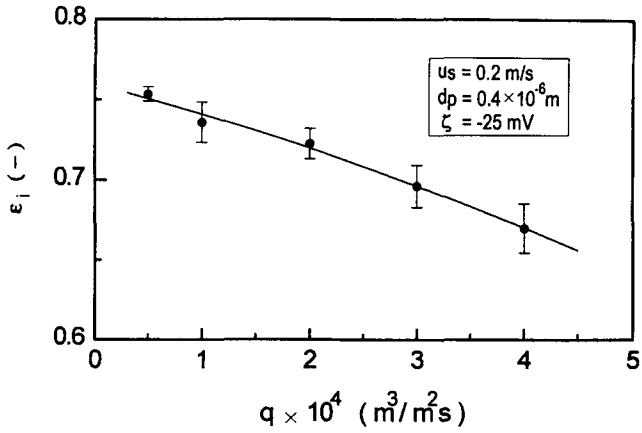

FIG. 16 Simulated packing porosity of particles under various filtration rates.

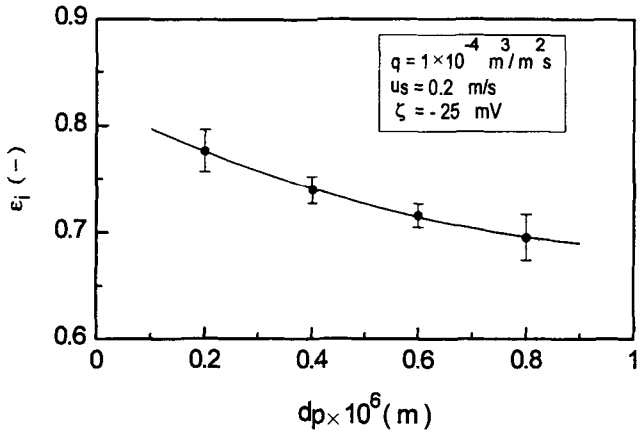

FIG. 17 Effect of particle size on simulated packing porosity of particles.

TABLE 1
A Comparison of Initial Filtration Rate of Crossflow Microfiltration between the Calculated Results and the Experimental Data (C_0 = 5 kg/m^3, ΔP = 4 × 10^4 N/m^2, T = 20°C, ζ = −25 mV, R_m = 1.12 × 10^{10} m^{-1})

	Run number				
	1	2	3	4	5
u_s (m/s)	0.6	0.4	0.2	0.6	0.6
d_p × 10^7 (m)	4	4	4	8	2.5
N_b × 10^3 (kg/m^2·s)[a]	3.04	4.27	5.87	2.98	3.1
t(s)	20	15	10	20	20
w_c × 10^2 (kg/m^2)[a]	6.08	6.41	5.87	5.96	6.2
ϵ (—)	0.63	0.63	0.62	0.53	0.66
α_{av} × 10^{-12} (m/kg)[b]	1.37	1.34	1.51	0.71	2.77
q_{cal} × 10^4 (m^3/m^2 s)[c]	4.23	4.12	4.03	7.47	2.19
q_{exp} × 10^4 (m^3/m^2 s)[d]	4.12	4.23	4.15	6.82	2.32
Deviation (%)[e]	2.67	−2.6	−2.89	9.53	−5.6

[a] Calculated by the proposed theory.

[b] $\alpha_{av} = \dfrac{180(1-\epsilon)}{\rho_s d_p^2 \epsilon^3}$.

[c] $q_{cal} = \dfrac{\Delta P}{\mu(w_c \alpha_{av} + R_m)}$.

[d] Measured by experiments.

[e] Deviation (%) = $\dfrac{q_{cal} - q_{exp}}{q_{exp}} \times 100\%$.

CONCLUSIONS

The Langevin equation has been adopted to trace the loci of submicron particles in laminar crossflow microfiltration. The effects of operating conditions on the particle trajectories have been discussed. It has been found that the Brownian motion of particles plays a more important role on particle migration under a smaller crossflow velocity of suspension or a smaller filtration rate. The estimated values of transported flux of particles arriving at the membrane surface increase with an increase of filtration rate and with a decrease of particle diameter; however, the crossflow velocity has no significant effect on the transported flux. The forces exerted on particles have been analyzed to estimate the probability of particle deposition on the membrane surface. The probability of particle deposition increases with an increase of the filtration rate, with a decrease of the crossflow velocity, with a decrease of the particle diameter, and with an increase of the zeta potential of particles. The packing structures of particles on the membrane surface at the initial stage of filtration have also been simulated. The porosity of the cake increases with an increase of the crossflow velocity, with a decrease of the filtration rate, and with a decrease of the particle diameter. The deviation between the calculated and experimental data of filtration rate at the initial period of filtration is less than 10% when the Reynolds number of the suspension flow is between 100 and 500.

ACKNOWLEDGMENT

The authors express their sincere gratitude to the National Science Council of the Republic of China for its financial support.

NOTATIONS

a	radius of particle (m)
A_H	Hamaker constant (—)
$A(t)$	Brownian random force per unit mass (m/s^2)
b	constant in Eq. (9) (—)
C_0	concentration of suspension (kg/m^3)
D	shortest distance between two particle surfaces (m)
d_p	diameter of particles (m)
e_0	absolute permittivity of free space ($C^2 \cdot J^{-1} \cdot m^{-1}$)
e_r	dielectric constant of the fluid between particles (—)
F_1	the component of the net force exerted on particle A whose direction is vertical to the connecting line between the two gravity centers of Particles A and B (N)

F_2 the component of the net force exerted on particle A whose direction is parallel to the connecting line between the two gravity centers of Particles A and B (N)
F_B Brownian force (N)
F_d frictional drag due to fluid flow (N)
F_e electrostatic force (N)
F_g gravity force (N)
F_i interparticle force (N)
F_l inertial lift force (N)
F_v van der Waals force (N)
g acceleration due to gravity (m/s^2)
H clearance of a filter (m)
L_f length of a filter (m)
m_p mass of a particle (kg)
N_b transported flux of particles ($kg/m^2 \cdot s$)
P probability of particle deposition (%)
ΔP filtration pressure (N/m^2)
q quasi-stationary filtration rate ($m^3/m^2 \cdot s$)
r particle position vector (m)
R_1 the integration defined in Eq. (19) (—)
R_2 the integration defined in Eq. (20) (—)
R_m filtration resistance of the filter membrane (m^{-1})
t filtration time (s)
u velocity of fluid (m/s)
u_s average velocity of suspension at the inlet of a filter (m/s)
V_e repulsive energy (J)
V_v van der Waals potential (J)
v_p velocity of particle (m/s)
v_l lift velocity of particle (m/s)
w_c mass of cake per unit area (kg/m^2)
x coordinate whose direction is parallel to the tangential flow of suspension (m)
y coordinate whose direction is vertical to the tangential flow of suspension (m)
y_b the y-coordinate of entering particles below which particles can be transported as they arrive at the membrane surface (m)

Greek Letters

α specific filtration resistance (m/kg)
ϵ porosity of cake (—)
ϕ wall correction factor of Stokes' law (—)
κ reciprocal of the thickness of the double layer (m^{-1})

λ	characteristic wavelength (m)
μ	viscosity of fluid (kg/s·m)
ν	kinematic viscosity of fluid (m^2/s)
ρ	density (kg/m^3)
Ψ_0	Stern potential (V)
τ_w	shear stress at wall of filter (N/m^2)
ζ	zeta potential of particles (V)

Subscripts

0	initial condition
av	average value of the properties for a filter cake
i	properties at the cake surface
s	solid
x	in the x-direction
y	in the y-direction

Superscript

*	dimensionless group

REFERENCES

1. M. Cheryan, *Ultrafiltration Handbook*, Ch. 4, Technomic Publishing Co., Pennsylvania, 1986.
2. G. Green and G. Belfort, "Fouling of Ultrafiltration Membranes: Lateral Migration and the Particle Trajectory Model," *Desalination*, *35*, 129 (1980).
3. A. L. Zydney and C. K. Colton, "A Concentration Polarization Model for the Filtrate Flux in Cross-Flow Microfiltration of Particulate Suspensions," *Chem. Eng. Commun.*, *47*, 1 (1986).
4. F. W. Altena and G. Belfort, "Laterial Migration of Spherical Particles in Porous Flow Channels: Application to Membrane Filtration," *Chem. Eng. Sci.*, *39*(2), 343 (1984).
5. E. Fischer and J. Raasch, "Cross-Flow Filtration," *Ger. Chem. Eng.*, *8*, 211 (1986).
6. W. M. Lu and S. C. Ju, "Selective Particle Deposition in Crossflow Filtration," *Sep. Sci. Technol.*, *24*(78), 517 (1989).
7. W. M. Lu and K. J. Hwang, "Cake Formation in 2-D Cross-Flow Filtration," *AIChE J.*, *41*(6), 1443 (1995).
8. G. C. Ansell and E. Dickinson, "Sediment Formation by Brownian Dynamic Simulation: Effect of Colloidal and Hydrodynamic Interaction on the Sediment Structure," *J. Chem. Phys.*, *85*, 4079 (1986).
9. G. C. Ansell and E. Dickinson, "Brownian Dynamic Simulation of the Fragmentation of a Large Colloidal Floc in Simple Shear Flow," *J. Colloid Interface Sci.*, *110*, 73 (1986).
10. G. C. Ansell and E. Dickinson, "Short-Range Structure of Simulated Colloidal Aggregates," *Phys. Rev.*, *A*, 1 (1987).

11. D. Gupta and M. H. Peter, "A Brownian Simulation of Aerosol Deposition onto Spherical Collectors," *J. Colloid Interface Sci.*, *104*, 357 (1985).
12. W. M. Lu, C. C. Lai, and K. J. Hwang, "Constant Pressure Filtration of Submicron Particles," *Sep. Technol.*, *5*, 45 (1995).
13. J. D. Sherwood, "The Force on a Sphere Pulled away from a Permeable Half-Space," *Physicochem. Hydrodyn.*, *10*, 3 (1988).
14. S. C. Ju, "A Study on the Mechanism of Cross-Flow Filtration," Ph.D. Dissertation, Department of Chemical Engineering, National Taiwan University, Taiwan, R.O.C., 1988.
15. P. Vasseur and R. G. Cox, "The Laterial Migration of Spherical Particle in Two Dimensional Shear Flow," *J. Fluid Mech.*, *78*, 385 (1976).
16. H. Sonntag and K. Strenge, *Coagulation Kinetics and Formation*, Chap. 1, Uplands Press, England, 1980.
17. R. J. Hunter, *Foundations of Colloid Science*, Ch. 7, Oxford University Press, New York, NY, 1987.

Received by editor December 20, 1996
Revision received April 1997